

Satellite-measured temporal variability of the Columbia River plume

Andrew C. Thomas^{*}, Ryan A. Weatherbee

School of Marine Sciences, University of Maine, Orono, ME 04469-5741, USA

Received 15 August 2005; received in revised form 18 October 2005; accepted 20 October 2005

Abstract

Six years (1998–2003) of SeaWiFS multispectral satellite data are used to document the seasonal and interannual variability of the Columbia River plume on the North American west coast. A supervised classification scheme using 5 channels of normalized water-leaving radiance (nLw at 412, 443, 490, 510 and 555 nm), with training pixels adjusted temporally to optimize the signature of plume core characteristics, quantifies the climatological seasonal location of 4 spectrally defined classes of surface water and provides estimates of variability in position as a probability. Winter plume orientation was northward and close to the shore, with infrequent adjustments to the south. Summer plume orientation was offshore and to the south, dissociated from the coast, with more frequent (>20%) occurrences of plume water and peripheral plume water (>50%) to the north. An effective characterization of interannual variability in plume dynamics is provided by time series of temporally averaged nLw at 555 nm, used as an estimate of suspended particulate material. Monthly means during maxima and minima in annual river discharge show the plume to be weakest both in spatial extent as well as absolute nLw values in 2001, a year of minimum river discharge. Time series of both (a) nLw 555 values at the river mouth and (b) Mode 2 of an empirical orthogonal function decomposition of the 6-year nLw 555 time series variance that isolates winter patterns are strongly correlated with river discharge. Interannual differences in monthly mean wind forcing are evident as changes in plume position during the winter, but at the 8-day and longer time scales examined here, summer interannual differences are dominated by differences in discharge volume.

© 2005 Elsevier Inc. All rights reserved.

Keywords: SeaWiFS; Columbia River plume; Seasonal variability; Interannual variability

1. Introduction

The Columbia River is the largest river on the west coast of North America, draining a region of approximately 665,000 km² with an average annual discharge of $\sim 260 \text{ km}^3 \text{ year}^{-1}$. The mouth of the river is at $\sim 46^\circ\text{N}$, entering the Pacific Ocean along a relatively straight and meridionally oriented coastline with a narrow shelf (Fig. 1). In a typical year, discharge is bimodal, with a winter peak, driven by the local seasonal maximum in precipitation, and a stronger spring–early summer peak driven by snowmelt at higher elevations within the watershed (Fig. 2). Winter discharge maxima are storm-driven and characterized by strongly episodic, short-lived (days) discharge peaks that are masked in the multi-year mean of Fig. 2. The spring freshet, averaging $\sim 12,000 \text{ m}^3 \text{ s}^{-1}$, is sustained over periods of months, is relatively consistent within

the year and in timing from year to year, but is less consistent in volume of discharge between years. Minimum discharge occurs during the later summer and early fall (August through October).

The plume from the Columbia River is one of the dominant hydrographic features of the California Current System (Hickey et al., 1998), traceable as a coherent, low salinity, tongue at least as far south as 38°N in summer. The plume region in the vicinity of the river mouth plays a key role in local shelf physical, biogeochemical and ecological functioning (Casillas, 1999; Garcia Berdeal et al., 2002; Hickey et al., 1998; Percy & Fisher, 1998; Stefansson & Richards, 1963), carrying a mixture of fine silts, clays and dissolved organic matter into the coastal zone. The plume influences nutrient concentrations and nutrient ratios in the surface layers, directly impacting the lowest trophic levels. Changes in stratification resulting from the freshwater input influence both vertical nutrient flux and the light regime in the upper mixed layer. Both dissolved and particulate material in the plume also influence the light regime. Local circulation patterns associated

^{*} Corresponding author.

E-mail address: thomas@maine.edu (A.C. Thomas).

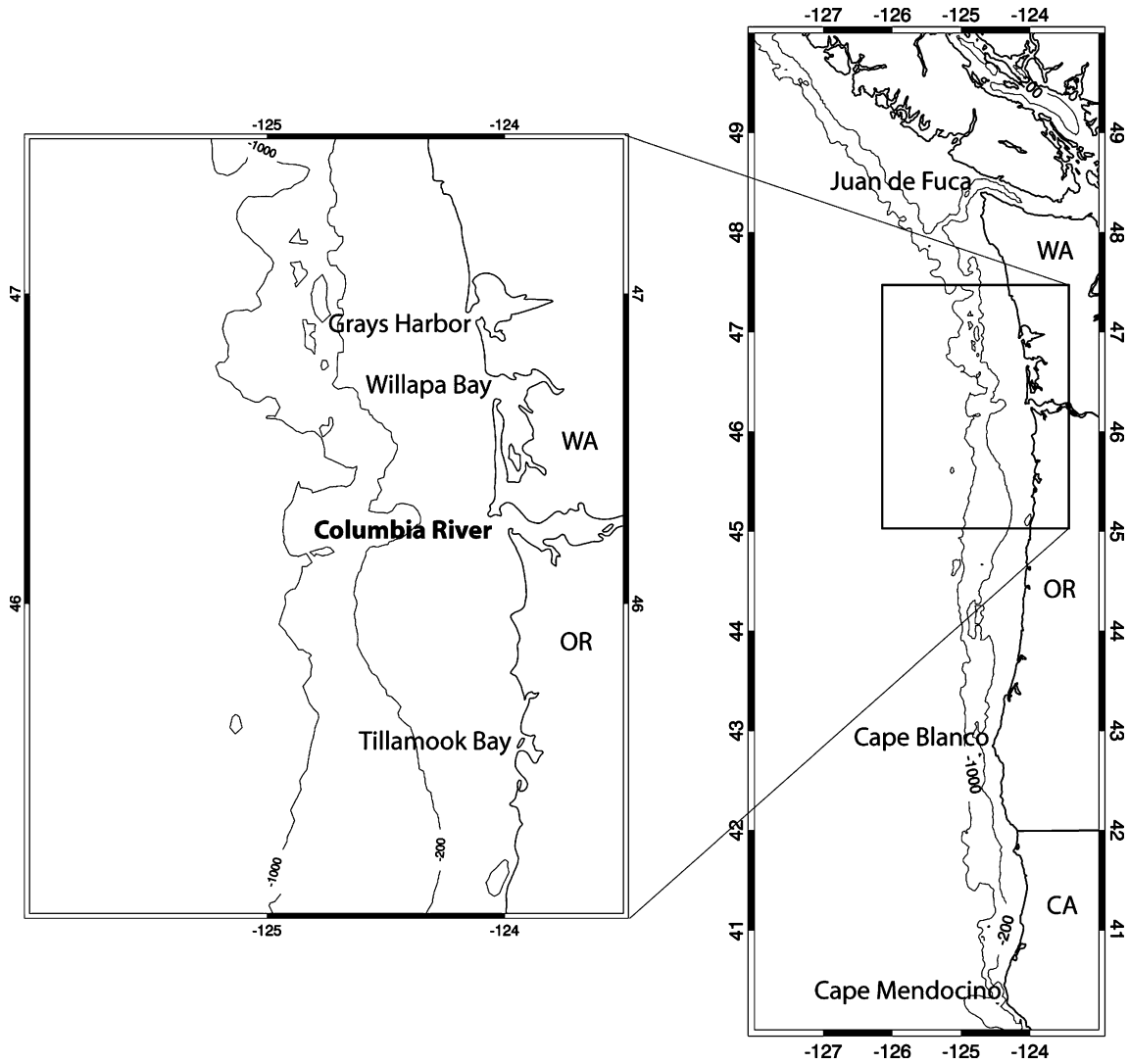


Fig. 1. The study area in the Pacific Northwest region of the USA, showing the Columbia River mouth, major geographic features of the region, the boundaries of the states of Washington (WA), Oregon (OR) and California (CA), and bottom bathymetry (m) on the continental shelf.

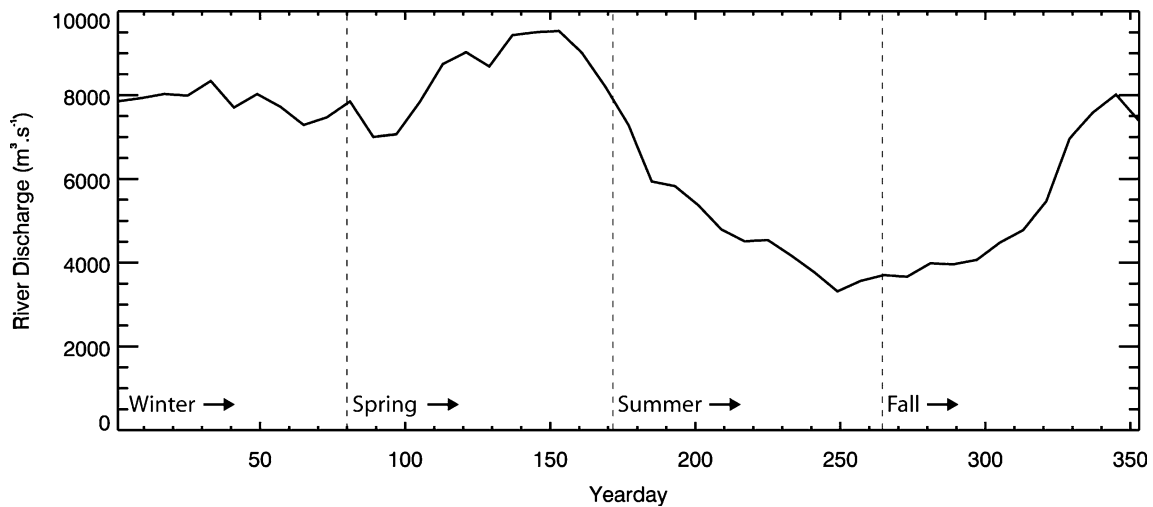


Fig. 2. The climatological mean Columbia River discharge volume, calculated from the 12-year mean of 8-day periods beginning January 1 in each year, showing a broad winter maximum, a second spring–early summer maximum and late summer minimum. The 8-day averages were calculated from daily data spanning 1992–2003. The 8-day periods were chosen to match the temporal averaging of the highest frequency SeaWiFS time series used in the study.

with the plume (e.g. geostrophic flows and frontal convergences) influence both vertical and horizontal transports. At higher trophic levels, enhanced primary productivity and frontal convergence zones provide a food source, and turbidity resulting from both riverine material and the enhanced phytoplankton concentrations provide a refuge from predation. The river plume region is thus a key nursery area for juvenile salmon as well as other species.

Theoretical flow considerations suggest that a river plume in the northern hemisphere should flow to the right (north in this case) under the influence of Coriolis forcing. In reality, the Columbia River plume is highly dynamic with a pronounced modulation by the local semidiurnal tide that has maximum spring tide ranges approaching 3 m in the estuary. Previous work has shown that the plume responds to local wind forcing almost instantly with changes of both position and thickness (Garcia Berdeal et al., 2002; Hickey et al., 1998). Modulation by both local current structure and wind forcing impose strong and well-understood seasonal differences in the position of the plume. In winter (approximately October–March), dominant alongshore wind forcing is northward, resulting Ekman transport in the upper ocean is onshore, and coastal near-surface currents are to the north. These act to reinforce rotational tendencies, and the dominant winter plume position is to the north, tightly along the Washington coast during strong wind events and more diffuse along the Washington mid-shelf during weaker winds (Hickey et al., 1998). In summer, dominant alongshore wind stress is to the south, resulting Ekman transport of the surface water column is offshore, and surface currents are to the south. The dominant summer plume is advected offshore and southward, separated from the coast, within the mean flow of the California Current. Transitions between these two regimes in the spring and fall can be relatively sudden, under the influence of local wind forcing (Strub et al., 1987). Superimposed on these two mean patterns are both event-scale processes that are capable of reversing climatological mean structure and interannual differences in both the timing and magnitude of wind and current patterns. Recent studies (Garcia Berdeal et al., 2002) show that even in summer, episodic relaxation or reversals of the prevailing equatorward wind stress allows the plume to influence the Washington shelf to the north to a larger extent than was previously thought.

Earlier satellite data views of the Columbia plume (Fiedler & Laurs, 1990) using NOAA AVHRR infrared data and Coastal Zone Color Scanner (CZCS) multispectral color data provides the basic seasonal spatial pattern characteristics of the plume off the Oregon/Washington coasts based on individual images of sea-surface temperature (SST) and pigment concentrations. Although aspects of the colour signal are non-conservative (e.g. chlorophyll and CDOM), in turbid conditions, the water-leaving radiance measured by ocean color satellites provides improved information on the location and/or movement of the upper water column compared to that measured in the infrared. Although both are limited by cloud cover, backscattered radiance in the visible part of the spectrum integrates over a deeper portion of the water column (several

meters) than the surface skin (few micrometers) measured by infrared. In addition, daily, seasonal and geographic changes in surface heat flux mean that there are times and places where the SST signal is an inadequate or biased tracer of upper water column dynamics. Although hampered by data gaps due to cloud cover, satellite data remain one of the most effective tools for monitoring the time/space patterns of turbid water (Binding et al., 2003; Figueras et al., 2004; Froidefond et al., 2002).

The launch of SeaWiFS in 1997 provided the first operational, multispectral capability to quantify aspects of plume behavior on a consistent basis over multiple years. Our purpose is to use the multi-year coverage of SeaWiFS data to provide a systematic quantification of the seasonal and interannual characteristics of the position and strength of the Columbia River plume and its variability. Issues of validation, calibration and quantitative comparisons of in-water constituents to satellite retrievals are beyond the scope of this manuscript. Here we focus on relative patterns of spectral signatures within the time series and utilize both multivariate and single channel approaches to document variability.

2. Data and methods

All available Level 1A SeaWiFS swaths intersecting the region 40°–50°N, 128.0°–123.5°W for the period of January 1998–December 2003 were downloaded from the Goddard Distributed Active Archive Center. These data were processed to Level 2 geophysical products using default NASA coefficients and community-standard algorithms as implemented by SeaDAS (version 4.5p1) and remapped to a cylindrical projection at 1.1 km resolution. The resulting product suite included normalized water-leaving radiances (nLw) at 412, 443, 490, 510, 555, 670, 765, and 865 nm, light attenuation at 490 nm (K490) (O'Reilly et al., 2000), and chlorophyll *a* concentration (OC4v4) (O'Reilly et al., 1998). Daily averages were calculated when more than one image occurred in a 24-h period. Daily data were further composited into 8-day and monthly means, as well as 8-day and monthly climatologies for the 6-year period, for all products. The study area was then subset from the images to geographic extents of 45.0°–47.5°N, 126.0°–123.5°W.

A supervised maximum likelihood classification procedure (e.g. Richards, 1993) applied to the 8-day multispectral composite time series was used to simplify seasonal differences in the spatial and temporal variation of surface water optical characteristics. Supervised classification requires that the desired output classes be trained using representative portions of the image to compile statistical properties of the spectrum of each class. After visual examination of a series of example scenes from different seasons, we subjectively trained on four of the most obvious optical water types: the immediate plume core itself, peripheral edges of the plume and inner shelf water, other shelf water, and offshore water. Training region polygons were manually drawn using false color composites (nLw 555 (red)/nLw 490 (green)/nLw 412 (blue)) as a guide (Fig. 3a), as this combination provided a visual guide of optical boundaries and regions better than any individual image product. A

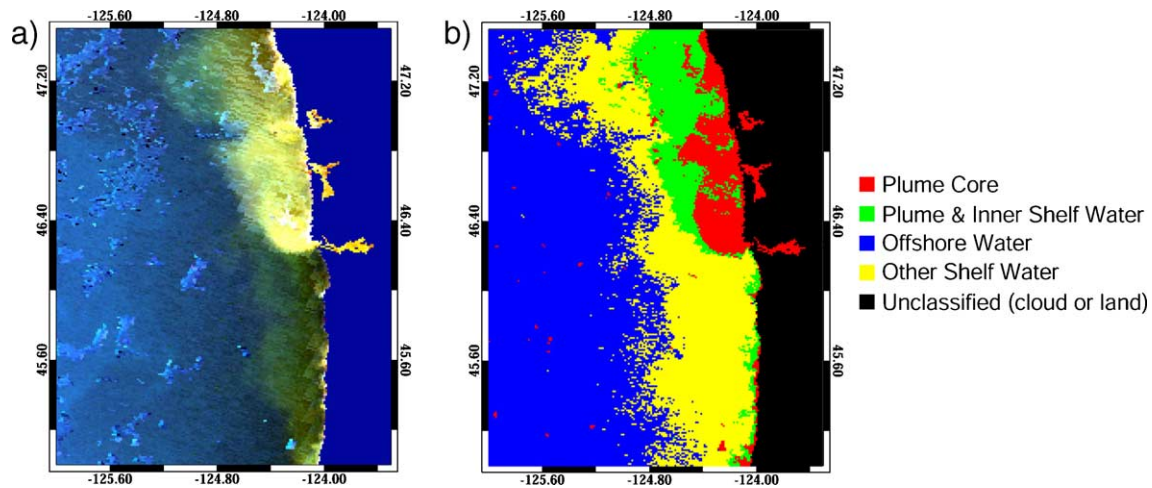


Fig. 3. (a) An example false color composite of SeaWiFS data (nLw 555 (red)/nLw 490 (green)/nLw 412 (blue)) of the study area showing the spatial pattern and spatial variability of the dominant shelf optical characteristics during a typical winter situation. (b) The same image after supervised maximum likelihood classification, separating four spectral classes of coastal water based on optical characteristics in 5 SeaWiFS channels. (For interpretation of the references to colour in this figure legend, the reader is referred to the web version of this article).

conservative approach was taken when defining training regions such that only areas that were obviously part of the four water types were included. Class training was performed on the first image in the time series (Jan 1–8, 1998 composite) using the criteria outlined in Table 1, followed by computation of the mean, standard deviation and covariance of the spectral signatures within each training polygon. These statistics, and the first five nLw bands (412–555), were used as input to the maximum likelihood routine. The result was an image containing pixels with only four possible values, each representing a possible optical water class (Fig. 3b). Once classification was completed, clouds and land were masked by setting any pixels with a value less than 0 in the chlorophyll product (which used the standard NASA cloud-masking routine) to an “unclassified” value in the class image.

Inspection showed that the spectral signature of the plume is highly variable between seasons and years, most likely due to temporally varying water column constituents contributing to the optical signature as well as varying thicknesses of the plume itself. A single set of spectral criteria, sufficient to consistently isolate the plume across the whole time series, resulted in class variance so broad that large regions of the shelf were often also classified as “plume”. This result occurred although the actual plume core and its position could be identified within the scene using stricter spectral criteria. A

single set of class statistics was therefore not adequate to capture temporal variability of the water types across seasons and years. As our goal was to follow the time-varying position of the river plume, we implemented a subjective, dynamic retraining protocol for the supervised maximum likelihood classification procedure. In this procedure, images in the time series following the training image were classified using the spectral signature statistics obtained from a previous image training set unless the result was obviously inconsistent with the patterns evident in the RGB image of the same data. When this occurred, retraining of the spectral characteristics using new polygon boundaries was done on the image. These new statistics were applied to the following images until inconsistencies with the RGB image were again evident. Training polygon area, therefore, varied for all classes over the time series depending on the size of the target region, cloud obstruction and clarity of features. On average, retraining was required every fourth composite (Table 2). This procedure was repeated until all 270 images in the time series were classified into our four classes. The mean spectral signature of all retrievals in the four classes across all 6 years of 8-day composites is shown in Fig. 4. As these means average across all seasons and years, variance about the means was large and not meaningful. Standard errors for means within scenes, however, were small. The range of standard errors observed across this time series associated with the means is reported in Table 3, smallest in offshore water and largest in the plume and

Table 1
Rules used to define supervised classification training regions

Optical water type	Training criteria
Plume core	Immediately off the mouth of the Columbia River, distinctly part of the initial plume
Plume and inner shelf water	Region(s) immediately peripheral to the Plume Core training polygon
Other shelf water	Region(s) near the coast that are not obviously associated with the plume
Offshore	Region(s) off the shelf with low nLw values in all three bands

Table 2
Number of class trainings required in each year of the time series

Year	Number of trainings
1998	11
1999	12
2000	8
2001	16
2002	9
2003	12

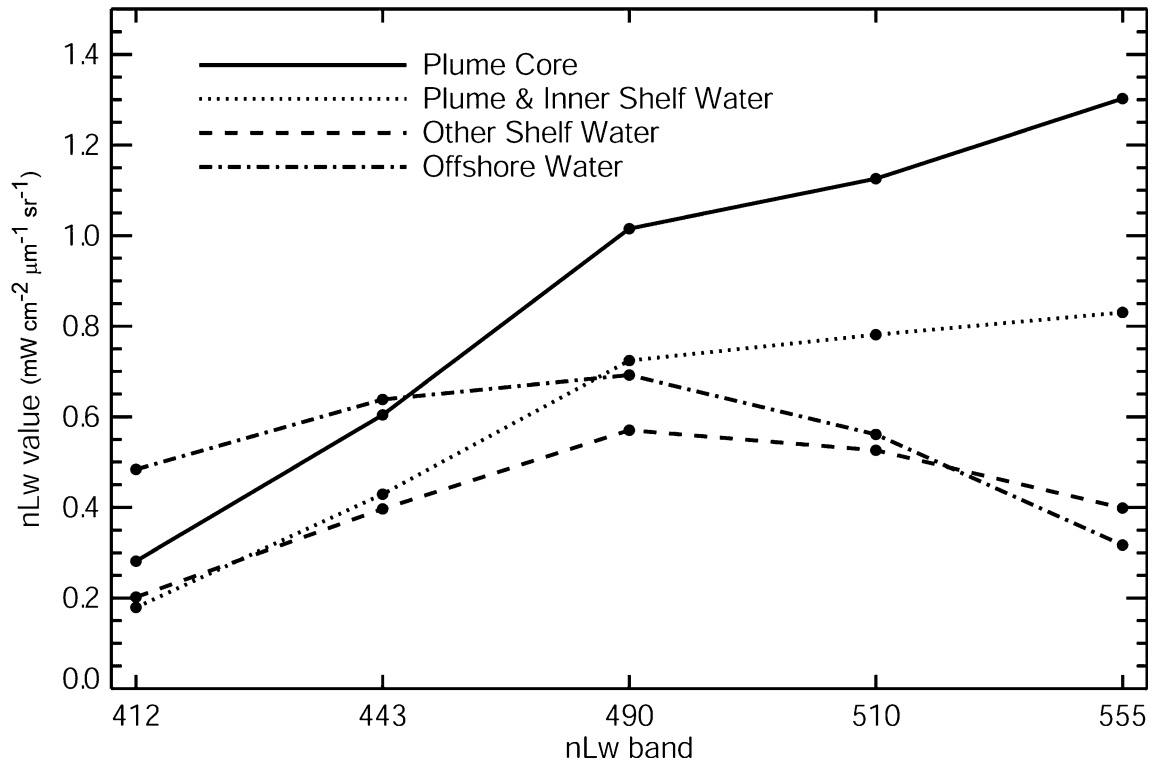


Fig. 4. The mean spectral signature of each of the four optical classes (Plume core, Plume and inner shelf water, Other shelf water and Offshore water) over the 6-year study period. Values at each wavelength were calculated by averaging the means of each 8-day image within the category over the 6-year period.

inner shelf class. The advantages of this retraining protocol are that the plume is isolated as a class even when its optical signature changes, i.e., it optimizes the definition and visualization of the plume position, and that images with cloud cover over critical class training regions can still be classified using temporally adjacent spectral statistics. A disadvantage is that information on interannual variability in optical signatures is lost.

Wind forcing for the study period was characterized using monthly average coastal Upwelling Index values obtained from the NOAA Pacific Fisheries Environmental Laboratory in Monterey, CA, for 45°N, 125°W. Their Upwelling Index is a model-derived product generated using U.S. Navy Fleet Numerical Meteorology and Oceanography Center sea level pressure fields. A time series of daily discharge from the Columbia River was obtained from the USGS using measurements from the Beaver Army Terminal, Quincy, OR (46°1055'N, 123°1050'W). Mean discharge values are based on a 24-h period, not tidal cycles. River flow at this location is

modulated by numerous upstream dams and downstream tidal currents but provides an excellent characterization of seasonal and interannual variability over the study period. Daily values were averaged into 8-day means for each year, matching the highest frequency used for analysis of the satellite data image series.

3. Results

3.1. Climatological seasonality

Inspection of the spatial distributions of the four water spectral classes resulting from the multispectral classification shows strong variability in time, even within a sequence of daily scenes. This pattern is consistent with both tide and wind being dominant forcing mechanisms (Hickey et al., 1998) and a typical temporal decorrelation scale for wind events of ~5 days in this area. The seasonal differences in spatial distribution of these spectral classes are summarized as a probability function,

Table 3

Range of nLw standard errors ($\text{mW cm}^{-2} \mu\text{m}^{-1} \text{sr}^{-1}$) in 8-day composites across all years for data within each of 4 classes defined by the maximum likelihood classification

nLw band	Plume core		Plume and inner shelf water		Other shelf water		Offshore water	
	Min	Max	Min	Max	Min	Max	Min	Max
412	0.002	0.15	0.0014	0.3	0.0009	0.10	0.0008	0.07
443	0.002	0.17	0.0013	0.2	0.0008	0.12	0.0007	0.05
490	0.002	0.15	0.0009	0.2	0.0007	0.13	0.0006	0.04
510	0.002	0.15	0.0010	0.17	0.0005	0.12	0.0005	0.04
555	0.002	0.20	0.0009	0.13	0.0004	0.13	0.0003	0.019

quantifying both dominant pattern and variability. Fig. 5 shows the occurrence rate at each grid location within the study area of the four spectral classes, divided between winter wind forcing conditions (northward dominant alongshore wind stress, onshore Ekman transport) and summer wind forcing conditions (southward dominant alongshore wind stress, offshore Ekman transport), summed over the 6-year study period. These climatological seasonal patterns quantify the two distinct modes of plume distribution, with seasonal differences in the variability about the dominant patterns. In winter, the plume core is angled north, along the Washington shelf, and remains closely associated with the inner shelf. Areas north of the mouth within 10 km of shore have over 50% of observations belonging to this spectral class. These data show that in winter, the plume core rarely (<10% of observations) extends further than 30 km offshore north of the river mouth and is rarely further than 10 km south of the mouth. The plume and inner shelf spectral class is also predominantly displaced north but is more diffuse in occurrence pattern. Highest occurrence percentages (~50–60%) are located 10–30 km offshore. Infrequent occurrences (>20%) of this class extend further south of the river mouth than the plume core, but still remain restricted to within ~50 km of the mouth. Other shelf water

occurs primarily south of the river mouth. The spatial pattern of winter occurrences of the offshore water spectral class parallel the coast (and bathymetry). The far western edge of the study area is occupied by offshore water for over 75% of observations. The isopleth marking 20% offshore class observations intrudes to within ~5 km of shore north of the river mouth and within 20 km of shore south of the mouth. During summer upwelling periods (Fig. 5), the plume core extends offshore, perpendicular to the coast with a strongly isometric distribution of >60% occurrence on all sides. In addition, summer patterns show that plume core occurrences of ~20% are spread over a much wider cross-shelf area (50–60 km offshore) than those of winter, and also occur south of the river mouth. This trend is also present in the plume and inner shelf spectral class. While maximum number of occurrences (~60%) are north of the river mouth and close to shore, occurrence rates of 50% are present in locations offshore and south of the river mouth. Both the plume core and the plume and inner shelf water classes show a summer pattern of elevated occurrence probability in a zone extending southwest from the river mouth. Summer occurrences of other shelf water >60% extend over the entire length of the coast study area, most frequent 5–80 km from shore south of the river mouth. North of the river mouth, increased

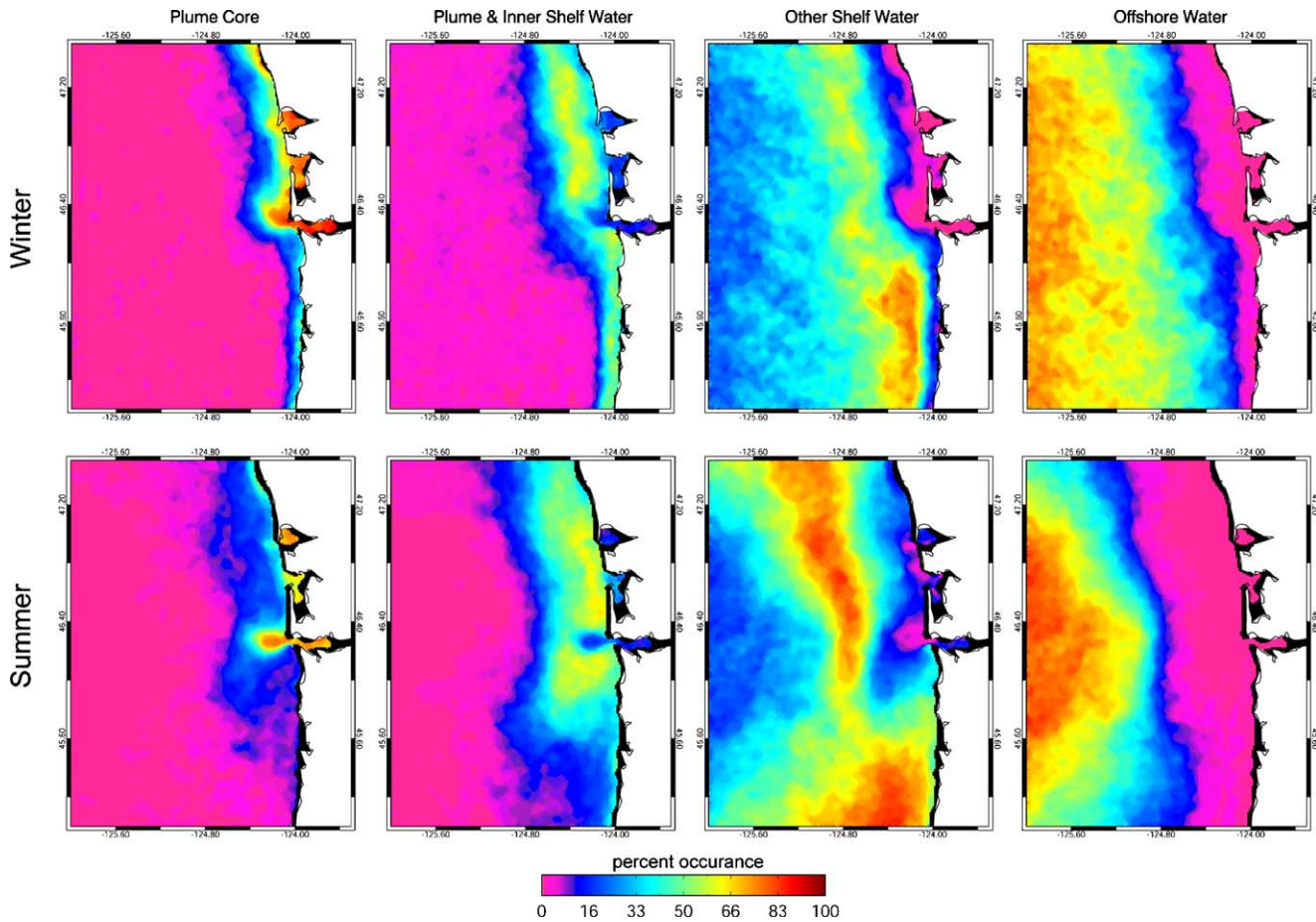


Fig. 5. Seasonal distribution of the four water spectral classes resulting from the supervised classification, showing the percent occurrence rate of the (1) Plume core, (2) Plume and inner shelf water, (3) Other shelf water and (4) Offshore water at each grid location. Seasons are determined by the dominant alongshore direction of wind forcing. Winter is defined as periods of persistent northward wind stress and onshore Ekman transport (downwelling conditions: Dec–Feb) and summer as those periods of persistent southward wind stress and offshore Ekman transport (upwelling conditions: Jun–Aug).

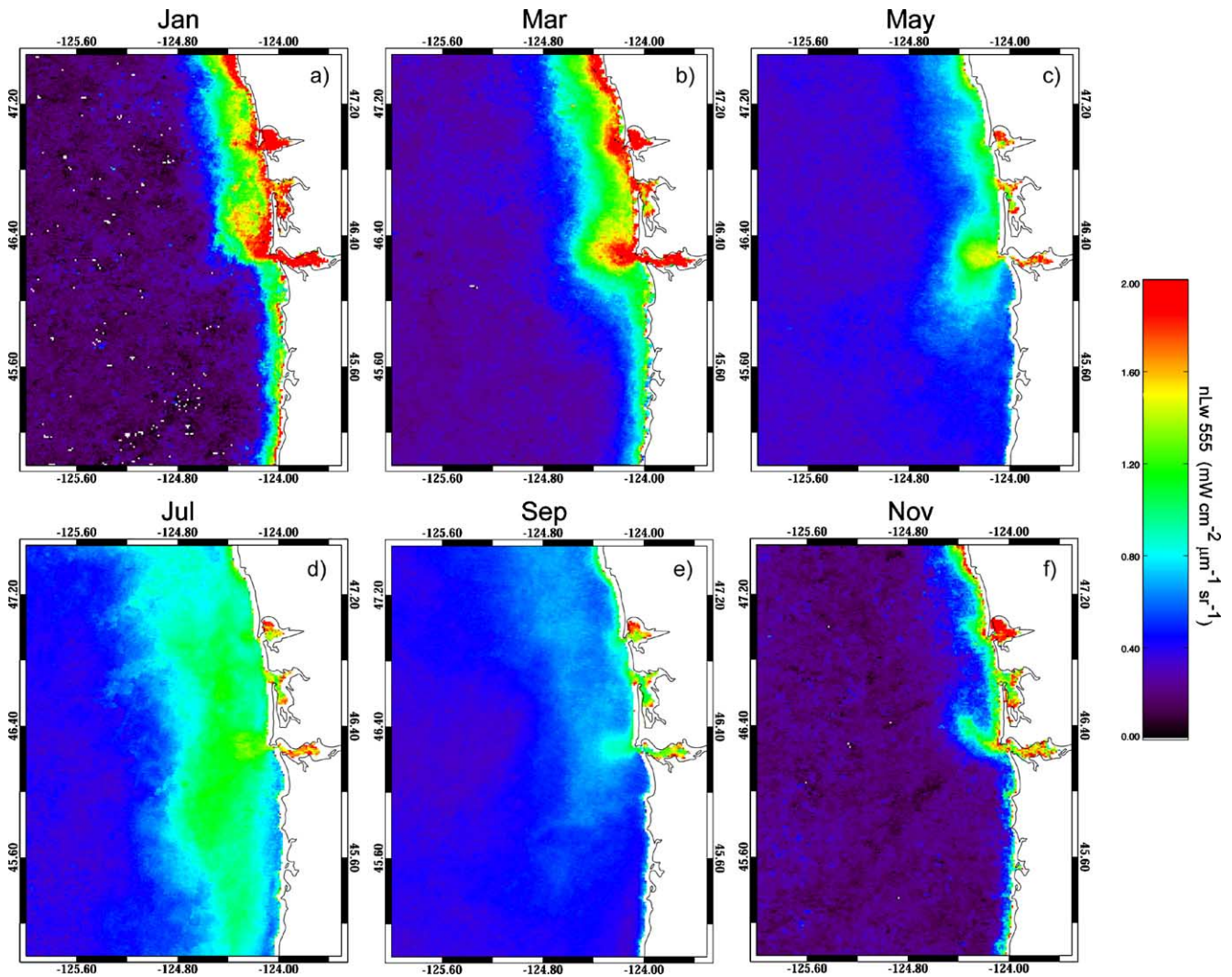


Fig. 6. The climatological (6 years) seasonal cycle of plume position evident in the normalized water-leaving radiance at 555 nm (nLw 555), an effective tracer of particulate matter in the water column. The time series show the progression in plume position and strength from (a) winter (January) through (b) spring (March), and into (c and d) summer (May, July), and then (e) fall (September) and (f) early winter (November).

occurrence percentages are restricted to a band centered considerably further (40–80 km) offshore than those evident in winter. During summer, the offshore water spectral class strongly dominates the westernmost center of the study area (>80% of observations). Occurrence rates >20% are displaced further offshore than in winter throughout the study area.

The seasonal progression in the position and size of the plume between the winter and summer situations described above is effectively illustrated by climatological (6-year mean) monthly time series of nLw 555 (Fig. 6), assumed to be an effective tracer of suspended particulate matter (Li et al., 2003). Values reflect the sum of both organic and inorganic material. In January, suspended matter from the plume is oriented strongly north along the Washington shelf and values $<0.2 \text{ mW cm}^{-2} \mu\text{m}^{-1} \text{sr}^{-1}$, characteristic of offshore regions, intrude within 20 km of shore along the Oregon shelf, beginning immediately south of the river mouth. In March, nLw values along the Washington coast remain higher and extend further offshore than those off Oregon, but elevated values within the plume core at the river mouth are isometric in distribution. By

May, offshore values have increased and plume/coastal values have decreased. However, the pattern of elevated values associated with the plume shows a pronounced southward displacement. In July, maximum values within the plume core are less than in earlier months, but the spatial pattern is spread over a wide region extending over 50 km offshore and both northward and southward to the edges of the study area. The highest values are evident south of the river mouth, along the Oregon shelf. Values are strongly reduced in September within the plume and over all shelf regions. The plume itself extends straight offshore with little evidence of bias either north or south. By November, offshore values have dropped, values within the plume are larger than those of September and the plume shows clear evidence of preferential northward advection onto the Washington shelf.

3.2. Interannual variability

Strongly correlated pictures of interannual variability in plume behavior were evident in multiple multi-spectral

products examined (K490, nLw in 5 channels). While presenting an optimized separation of plume water from other optical classes in each scene, the temporal adjustment of training sets in the supervised classification removes a clear signal of interannual variability from the results. Here we present the picture of interannual variability afforded by monthly composites of nLw 555, using three example months that represent seasonal extremes in river discharge and wind forcing.

February nLw 555 patterns over the 6-year period (Fig. 7) represent conditions during the winter maximum in discharge and winter wind forcing (northward, onshore Ekman transport). The plume signature is strongest (nLw values and spatial extent of higher values) in 1998, 1999 and 2003 (nLw 555 > 2.0 mW cm⁻² μm⁻¹ sr⁻¹) and relatively weak in 2001. Spatial patterns indicate that the plume was oriented strongly to the north and close to the Washington shelf in 1998 and 1999, most strongly so in 1999. Both 2000 and 2002 show dominant, but weaker, northward orientation and an increased offshore distribution. The weak plume in 2001 and the strong plume in 2003 each extend westward, orientations similar to those expected during summer wind forcing conditions (Fig. 5 and Fiedler & Laurs, 1990). May nLw 555 patterns over the 6-year period (Fig. 7) represent conditions during the spring maximum in discharge and after the wind has switched to summer conditions of dominant southward alongshore stress and offshore Ekman transport. The plume is strongest in 1998 and 1999 (nLw 555 > 1.5 mW cm⁻² μm⁻¹ sr⁻¹) and relatively weak in 2001. In each year, the main core of the plume extends westward, perpendicular to the shore. Southerly displacement of the offshore portions of the plume is evident in each year except 2000, most strongly in 1998, 1999 and 2002. In both 1998 and 2000, the imagery shows evidence of northward displacement at times during the month. Elevated values of nLw 555 along the Washington shelf are also evident in 1999, however, the pattern is not as obviously directly spatially connected with the river mouth. Patterns during September (Fig. 7) represent late summer, minimum river discharge conditions, during summer wind conditions of predominantly southward stress and offshore Ekman transport. In all years, September values of nLw are lower (usually < 1.0 mW cm⁻² μm⁻¹ sr⁻¹) and the plume is less well defined than at other times of the year. Over the 6-year period, the plume is weakest in 2001. In both 1999 and 2002, particulates within the water column over the shelf that are not obviously associated with plume discharge have high nLw 555 values. These patterns, most likely backscatter from phytoplankton, are also strongly evident in other summer months (July–August, not shown) when upwelling, nutrient enrichment of the shelf and primary productivity is strong. In each year, the September plume orientation is westward, perpendicular to the coast, consistent with expected summer patterns.

Overall temporal variability of the plume in the complete time series is effectively summarized using an empirical orthogonal function (EOF) decomposition (principal component analysis) of the 6-year monthly image sequence of nLw 555. An EOF decomposes a time- and space-varying signal

into orthogonal modes with the first mode containing the largest portion of the variance and successive modes containing decreasing variance. Each mode is represented by a space pattern and a time series describing the modulation of that pattern over the study period. The first two modes of the EOF decomposition (Fig. 8a) represent over 52% of the total variance. Variance decreased rapidly in higher modes with only 6% in the third mode (not shown). The space pattern associated with Mode 1 shows a maximum offshore of the river mouth, extending in an alongshore pattern approximately between the 100 and 200 m isobaths, both north and south of the mouth. Highest values and largest spatial extent are to the south, suggestive of summer patterns (Fig. 5). The time series associated with Mode 1 confirms this pattern is maximum in summer and minimum in early winter in each year. The strongest signals of interannual variability apparent in the time series are (i) maxima in the summers of 1998 and 1999, (ii) the strongest and most prolonged negative period in late 2000 through the first half of 2001, followed by (iii) a summer maximum in 2001 of the shortest duration in the time series (using values > 0 as an index). The space pattern in the second strongest mode (Fig. 8b) shows a strong cross-shelf gradient, maximum nearshore over the entire study area. Maximum values and largest cross-shelf extent is north of the river mouth. Mode 2 isolates variance in plume patterns advected north along the Washington shelf, suggestive of a winter plume pattern (Fig. 5) and nearshore turbidity, likely associated with resuspension in shallow areas during winter storms. The time series of this mode shows maxima during winter months and minima during summer for this pattern. The clearest signals of interannual variability in the time series are the strongest peak in the winter of 1998–1999 and the weakest peak in winter of 2000–2001.

4. Discussion

Beyond the obvious differences in seasonal mean position of the plume, seasonal differences in variability of the plume position are also documented effectively in Fig. 5. Variability results from the occurrence of episodic wind events during both seasons that provide forcing counter to the seasonal mean conditions. During summer upwelling conditions, when the dominant plume orientation is offshore and wind and current forcing is to the south, both the plume core and plume-inner shelf spectral water classes have occurrence rates to the north of the river mouth, along the Washington shelf, of up to 20% and >50%, respectively. This is consistent with hydrographic records showing plume water in summer off the Washington shelf (Hickey et al., 2005). In comparison, occurrence of plume spectral classes south of the river mouth during winter conditions (Fig. 5) is relatively rare. Winter variability in Fig. 5 is primarily manifest as differences in cross-shelf position off Washington, observations that are consistent with winter salinity fields shown by Hickey et al. (1998). Model results (Garcia Berdeal et al., 2002) show that due to the anticyclonic rotational tendency of the plume, stronger winds of longer duration are required in winter to

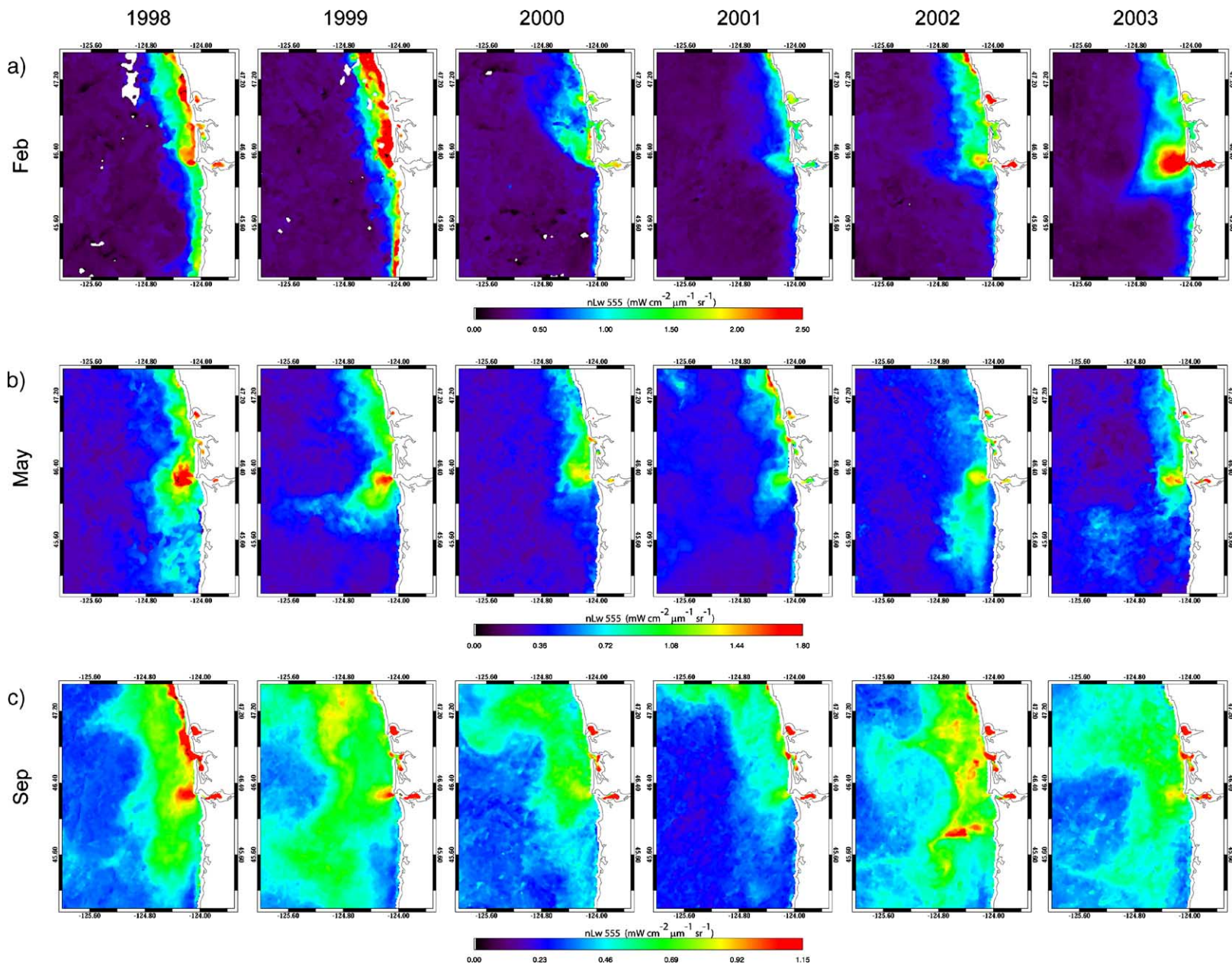


Fig. 7. Interannual variability in plume position and character in the normalized water-leaving radiance at 555 nm (nLW 555) over the 6-year study period for monthly means in each year of (a) February, (b) May and (c) September. Note changes in scale.

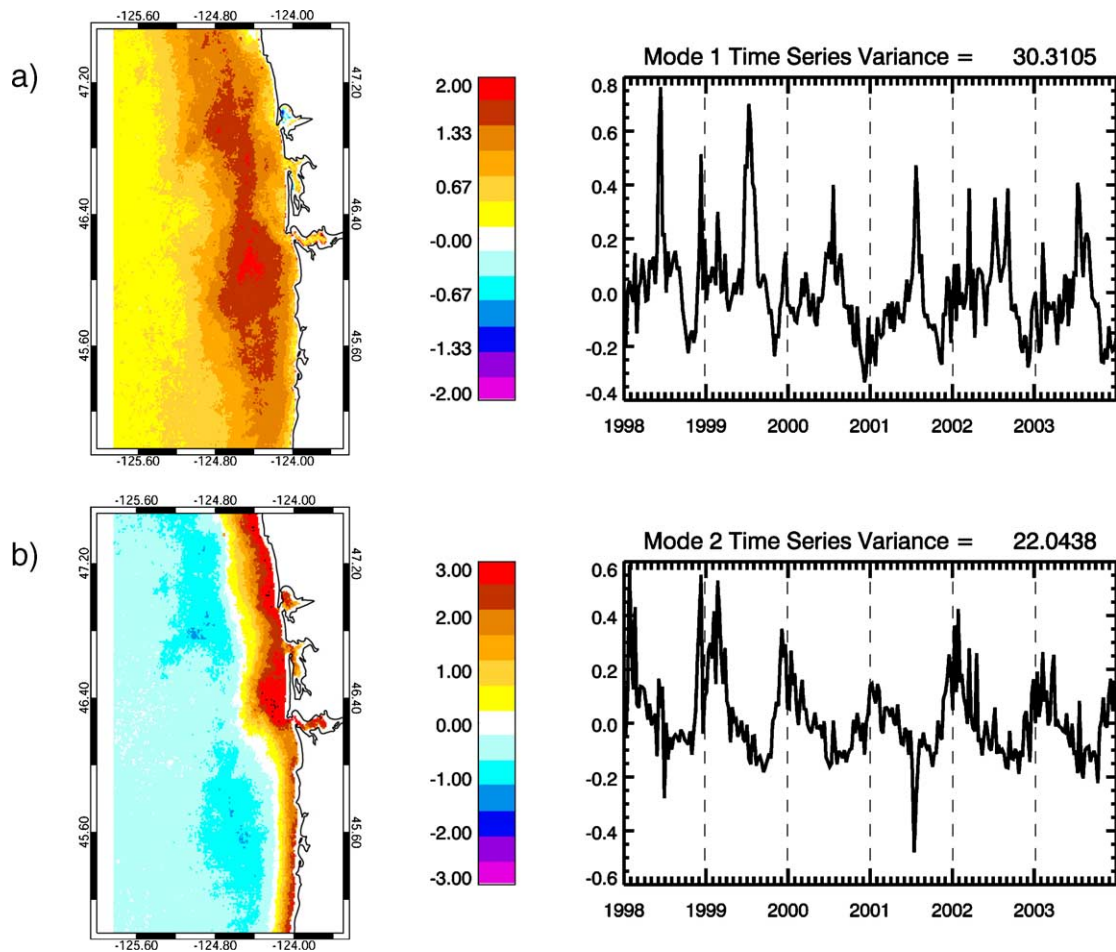


Fig. 8. Results of the EOF decomposition of 6-year monthly time series of nLw 555, showing the dominant mode (a), and the second strongest mode (b), which, together, explain over 52% of the total variance. Each mode consists of a space pattern (left) and the time series (right) showing the temporal modulation of the space pattern. The first two modes effectively divide dominant patterns between those of summer (Mode 1) and those of winter (Mode 2), highlighting interannual variability in the strength of these patterns.

reverse the plume orientation. In summer, episodic northward wind events or even relaxation of the upwelling-favorable southward winds are assisted by Coriolis, making summer displacement to the north more frequent than winter displacement to the south. Although differentiating the plume from turbid water resulting from local resuspension or discharge from other Washington bays is not possible, the 20–50% occurrence rates of plume water off Washington during summer evident in Fig. 5 are entirely consistent with those reported by Hickey et al. (2005).

The strongest signal of interannual variability in Figs. 7 and 8 is a relatively weak plume (values within the plume core and overall size) in winter 2000–2001 and summer 2001. The winter of 2000–2001 was characterized by strong negative anomalies in precipitation over the Pacific Northwest. This resulted in both weak winter discharge from local precipitation and weak summer discharge from the reduced snowpack at higher elevations. Fig. 9 shows Columbia River discharge averaged into 8-day periods over the 6-year study period. Reduced discharge peaks during both winter and spring periods in 2001 are clearly evident. The reduced river discharge is consistent with the weak plume evident in monthly

means for February (winter), May (spring) and September (late summer) in Fig. 7 and also the relative duration of the summer maximum in Mode 1 (primarily summer patterns) of the EOF in Fig. 8. The discharge time series in Fig. 9 is strongly correlated with both the time series from EOF Mode 2 (winter patterns) and also a time series of nLw 555 values (Fig. 9) subsampled and spatially averaged over a 30 km² region off the mouth of the river (centered at 46.24°N, 124.13°W). Although not quantified here, the latter time series is indicative of changes in the suspended material concentration at the mouth (Froidefond et al., 2002). Also evident in the discharge time series (Fig. 9) is the relatively strong maximum during the anomalously wet winter of 1998–1999. This maximum is associated with a maximum in the satellite-derived time series shown in Fig. 8 (Mode 2, primarily winter patterns) and the nLw 555 time series from the plume core (Fig. 9). In the absence of comprehensive concurrent in situ data, we are unable to calculate units of turbidity. However, these data show that the SeaWiFS time series is well suited to quantifying relative changes in both suspended matter and plume position that are indicative of important interannual changes in volume discharge.

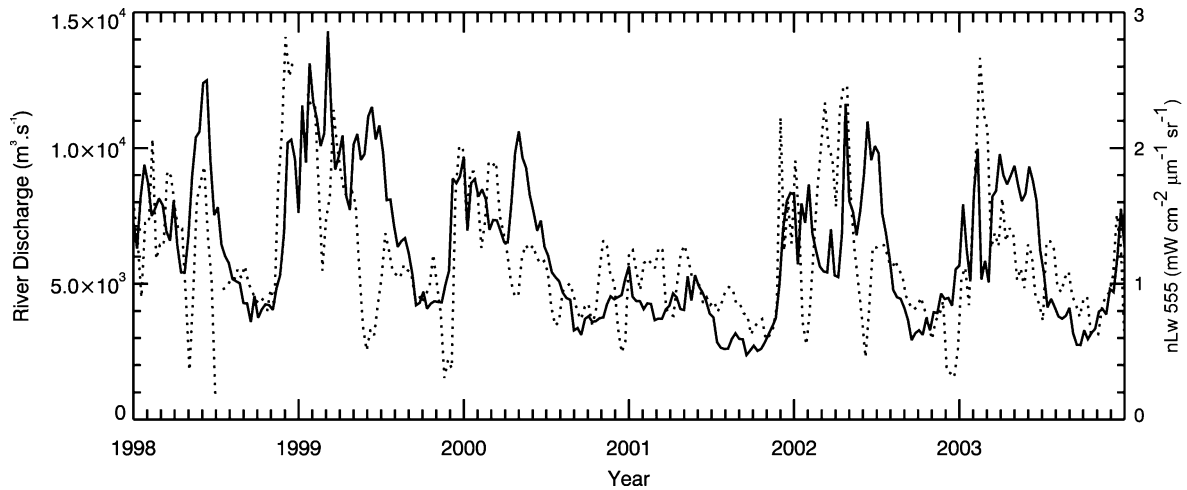


Fig. 9. Time series of Columbia River discharge for 1998–2003 (solid line), averaged into 8-day periods from daily measurements near the river mouth at Quincy, OR. Also shown is a time series of nLw 555 (dashed line) averaged over a 30 km² region immediately offshore of the river mouth, sampled from 8-day composite images.

Previous work has shown that the plume responds quickly (hours to days) to changes in wind forcing (Hickey et al., 1998). Here we focus on wider time window averages to view interannual differences. Fig. 10 characterizes wind forcing as anomalies in the monthly mean upwelling index over the study period. The climatological seasonal cycle of upwelling index for the area is also shown, for reference. The strongest anomalies are present during winter months associated with storm events. The strongest of these is the downwelling of February 1999. Fig. 9 shows that storms in this month also created a maximum in river discharge. Comparison of February monthly means in nLw 555 (Fig. 7) shows that 1999 is characterized by a plume pattern that is (1) strongly oriented to the north, (2) closely pushed onto the Washington shoreline and has (3) among the strongest nLw values in the time series. Conversely, wind forcing in 2003 is the weakest February in our study period and the plume

pattern does not show strong northward orientation. In 2003, the plume pattern is offshore, directly west, more similar to summer patterns than other February patterns. A qualitative comparison among the 6 available February means shows that the 2 winters of strongest negative wind anomalies (strongest northward forcing), 1998 and 1999, both had plume patterns oriented most strongly to the north. Three years of weakest February northward forcing (2001, 2002 and 2003) have plume patterns that have a stronger west, offshore orientation with weaker evidence of northward orientations. Wind anomalies during May do not have strong interannual variability within our 6-year study period. Interannual differences in wind forcing are stronger in September than in May, with strongest offshore Ekman transport (southerly winds) in 1998 and 1999, both years of relatively strong offshore and westward-oriented plume patterns (Fig. 7).

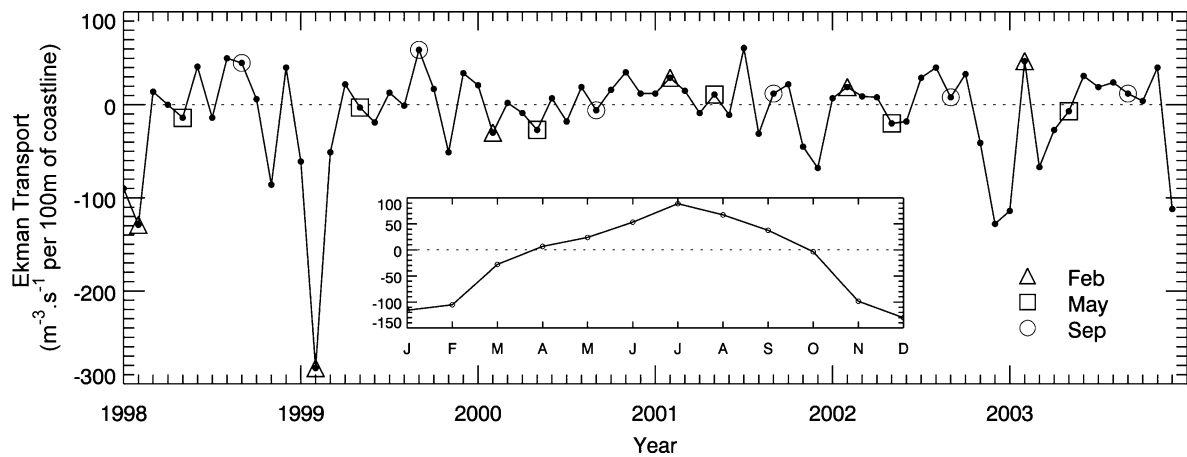


Fig. 10. Monthly anomalies of cross-shelf Ekman transport (positive offshore) at 45°N over the study period, characterizing the dominant, alongshore, component of coastal wind forcing. Transport values are an Upwelling Index, made publicly available by the National Oceanic and Atmospheric Administration at <http://www.pfeg.noaa.gov>. Anomalies are calculated as differences from a 30-year climatology for each month. This climatology (insert) shows the mean seasonal cycle of negative cross-shelf transport (onshore, downwelling) conditions during winter, resulting from dominant northward alongshore wind stress, to positive (offshore, upwelling) conditions in summer, resulting from dominant southward alongshore wind stress.

5. Conclusions

Here we provide a preliminary view of the ability of multispectral ocean color satellites to monitor the size and position of the Columbia River plume on seasonal and interannual time scales. The plume follows patterns expected based on previous in situ data from moorings and cruises. The satellite data are able to provide a systematic analysis over multiple seasons and years and add a more complete two-dimensional picture of the plume pattern. The plume extends north in the winter under the influence of northward wind stress, closest to the Washington coast during periods of maximum wind forcing. During summer, the plume extends offshore and south, usually dissociated from the coast, under the influence of dominant southward winds and offshore Ekman transport. Variability about these seasonal patterns is more frequent in summer than winter, with summer occasions of plume water extending northward off the Washington coast in 20–50% of the available observations, depending on the optical signature used to trace it. Interannual differences in the plume pattern evident in satellite data are strongly related to differences in river discharge. Interannual differences associated with wind forcing are most clearly evident in winter, when anomalies are strongest as storm events propagate through the region.

Interannual differences in the strength and position of the Columbia River plume have a strong influence in the Washington–Oregon shelf ecosystem through sediment deposition, nutrient concentrations and its affect on circulation and stratification. Additionally, the plume is an important juvenile salmon habitat, both as a refuge and food source. Quantitative relationships between the satellite-measured signal and in situ optical properties to derive in-water biogeochemical values, as has been done in other study regions (e.g. Binding et al., 2003; Froidefond et al., 2002; Myint & Walker, 2002), requires a dedicated field program and resulting data set for comparison. In the absence of access to such a data set, we provide analyses of the relative pattern. Our results show that the time series is well suited to extracting numerous metrics of relative interannual variability in plume size, position and signature relevant to fisheries and coastal management. Future efforts to collect co-incident in situ data will result in a quantitative assessment of plume dynamics in biogeochemical units, further increasing the utility of satellite multispectral data in monitoring the position, strength and character of the Columbia River plume and increasing their value as a local ecological monitoring tool.

Acknowledgements

We thank the SeaWiFS team at Goddard Space Flight Center for their groundbreaking efforts in making large datasets and processing tools so readily available to the community. We

thank Collin Roesler and Emmanuel Boss for helpful discussions on optical considerations and Bill Peterson and Ed Casillas for helpful discussions on plume dynamics and ecological implications. Funding for this work was provided by NSF and NASA through grant OCE-0000899. This is contribution number 263 of the U.S. GLOBEC program.

References

- Binding, C. E., Bowers, D. G., & Mitchelson-Jacob, E. G. (2003). An algorithm for the retrieval of suspended sediment concentrations in the Irish Sea from SeaWiFS ocean colour satellite imagery. *International Journal of Remote Sensing*, 24(19), 3791–3806.
- Casillas, E. (1999). Role of the Columbia River estuary and plume in salmon productivity. In G. A. Bisbal (Ed.), *Ocean conditions and the management of Colombia River salmon; proceedings of a symposium*. Portland, OR: Northwest Power Planning Council.
- Fiedler, P. C., & Laurs, R. M. (1990). Variability of the Columbia River plume observed in visible and infrared satellite imagery. *International Journal of Remote Sensing*, 11(6), 999–1010.
- Figueras, D., Karnieli, A., Brenner, A., & Kaufman, Y. J. (2004). Masking turbid water in the southeastern Mediterranean Sea utilizing the SeaWiFS 510 nm spectral band. *International Journal of Remote Sensing*, 25(19), 4051–4059.
- Froidefond, J.-M., Lavender, S., Laborde, P., Herbland, A., & Lafon, V. (2002). SeaWiFS data interpretation in a coastal area in the Bay of Biscay. *International Journal of Remote Sensing*, 23(5), 881–904.
- Garcia Berdeal, I., Hickey, B. M., & Kawase, M. (2002). Influence of wind stress and ambient flow on a high discharge river plume. *Journal of Geophysical Research*, 107(C9), 3130. doi: 10.1029/2001JC000932.
- Hickey, B. M., Geier, S. L., Kachel, N. B., & MacFadyen, A. (2005). A bi-directional river plume: The Columbia in summer. *Continental Shelf Research*, 25(16), 1631–1656.
- Hickey, B. M., Pietrafesa, L. J., Jay, D. A., & Boicourt, W. C. (1998). The Columbia River plume study: Subtidal variability in the velocity and salinity fields. *Journal of Geophysical Research*, 103(C5), 10339–10368.
- Li, R.-R., Kaufman, Y. J., Gao, B.-C., & Davis, C. O. (2003). Remote sensing of suspended sediments and shallow coastal waters. *IEEE Transactions on Geoscience and Remote Sensing*, 41(3), 559–566.
- Myint, S. W., & Walker, N. D. (2002). Quantification of surface sediments along a river dominated coast with NOAA AVHRR and SeaWiFS measurements: Louisiana, USA. *International Journal of Remote Sensing*, 23(16), 3229–3249.
- O'Reilly, J. E., Maritorena, S., Mitchell, B. G., Siegel, D. A., Carder, K. L., Garver, S., et al. (1998). Ocean color chlorophyll algorithms for SeaWiFS. *Journal of Geophysical Research*, 103, 24937–24954.
- O'Reilly, J. E., Maritorena, S., O'Brien, M. C., Siegel, D. A., Toole, D., Menzies, D., et al. (2000). SeaWiFS postlaunch calibration and validation analyses: Part 3. *NASA Technical Memorandum*. 2000-206892, 11, 49.
- Pearcy, W. G., & Fisher, J. P. (1998). Migrations of coho salmon, *Onchorhynchus kisutch*, during their first summer in the ocean. *Fish Bulletin*, 86, 173–195.
- Richards, J. A. (1993). *Remote sensing digital image analysis* (p. 340). New York: Springer-Verlag.
- Stefansson, U., & Richards, F. A. (1963). Processes contributing to the nutrient distributions off the Columbia River and Strait of Juan de Fuca. *Limnology and Oceanography*, 8(4), 394–410.
- Strub, P. T., Allen, J. S., Huyer, A., & Smith, R. L. (1987). Large-scale structure of the spring transition in the coastal ocean off western United States. *Journal of Geophysical Research*, 92, 1527–1544.